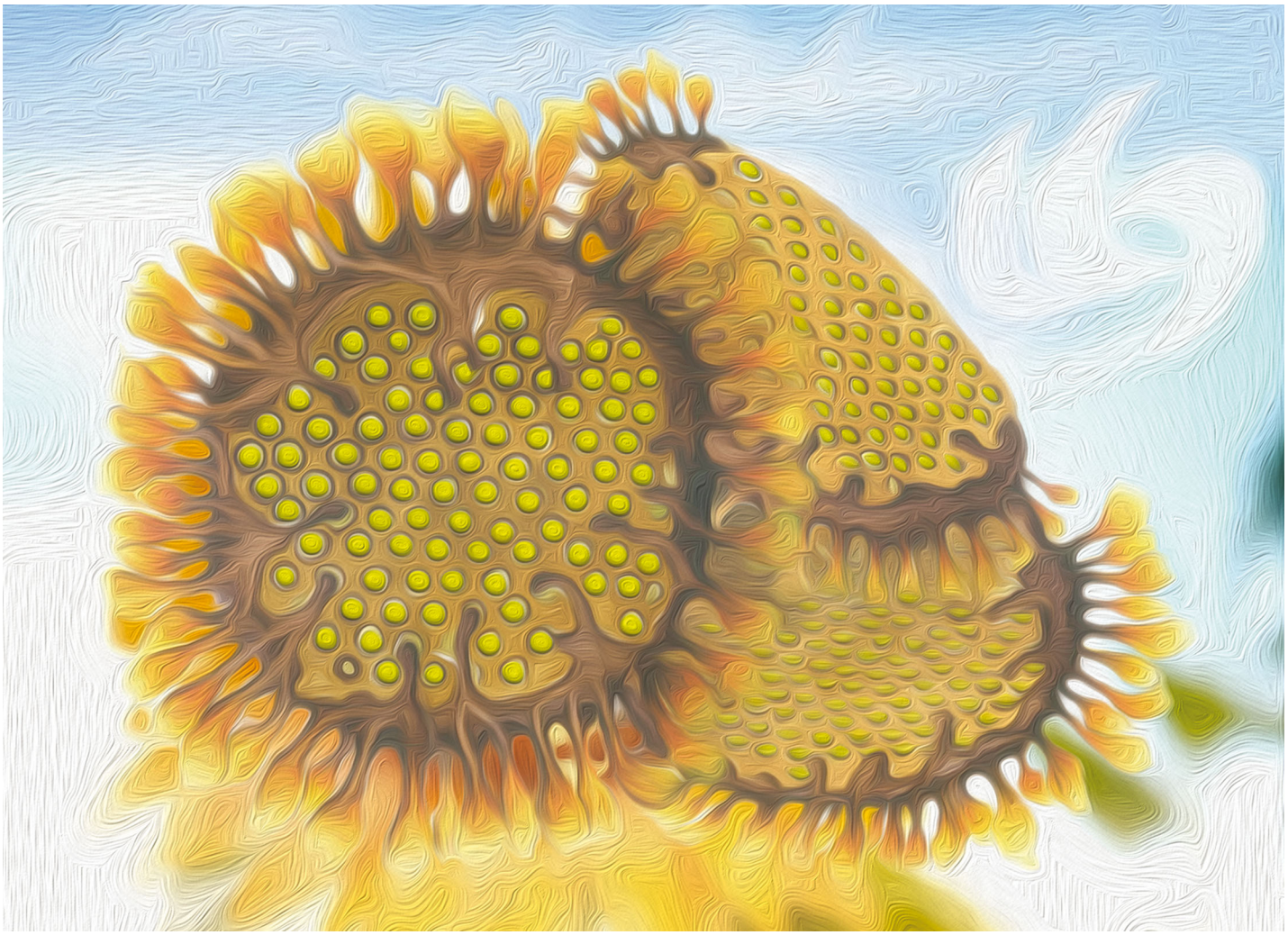

**Showcasing research from the State Key Laboratory of Advanced Technology for Materials Synthesis and Processing, Wuhan University of Technology, Wuhan, China.**

High viscosity to highly dispersed PtPd bimetallic nanocrystals for enhanced catalytic activity and stability

A facile high-viscosity-solvent method has been developed to synthesize PtPd bimetallic nanocrystals highly dispersed within various mesostructures. These highly dispersed PtPd bimetallic nanocrystals exhibit high catalytic activity, stability and durability in both the hydrogenation of nitrobenzene and oxygen reduction reaction.

## As featured in:


See Xiao-Yu Yang, Bao-Lian Su *et al.*, *Chem. Commun.*, 2016, **52**, 8219.

ROYAL SOCIETY OF CHEMISTRY

www.rsc.org/chemcomm

Registered charity number: 207890

ChemComm

COMMUNICATION

View Article Online
View Journal | View Issue



Cite this: *Chem. Commun.*, 2016, 52, 8219

Received 29th January 2016,
Accepted 16th May 2016

DOI: 10.1039/c6cc00912c

www.rsc.org/chemcomm

# High viscosity to highly dispersed PtPd bimetallic nanocrystals for enhanced catalytic activity and stability†

Jie Ying,[a] Zhi-Yi Hu,[b] Xiao-Yu Yang,*[a] Hao Wei,[a] Yu-Xuan Xiao,[a] Christoph Janiak,[c] Shi-Chun Mu,[a] Ge Tian,[a] Mu Pan,[a] Gustaaf Van Tendeloo[b] and Bao-Lian Su*[ad]

**A facile high-viscosity-solvent method is presented to synthesize PtPd bimetallic nanocrystals highly dispersed in different meso-structures (2D and 3D structures), porosities (large and small pore sizes), and compositions (silica and carbon). Further, highly catalytic activity, stability and durability of the nanometals have been proven in different catalytic reactions.**

High dispersion of metal nanocrystals are the most effective and best-known way to enhance the activity, stability and durability of nanometals.[1–5] Although certainly promising, obtaining highly dispersed nanometals in various nanostructured architectures is still a great challenge, and many critical issues should be addressed for their practical applications, such as low cost, fast kinetics, high stability and durability.[6–9] There have been many successful routes to synthesize uniform nanometals in meso-structured supports, such as ion exchange/wetness impregnation,[10,11] *in situ* encapsulation,[12,13] and organometallic introduction.[14,15] With more requirements of highly dispersed nanometals in practical applications, further progress has been made. One of the techniques is surface functionalization of meso-channels *via* organic modification,[16,17] resulting in size uniformity and a high dispersion of nanometals, in spite of the high cost of post-synthesis and instability of the organic layers under thermal and solvent conditions. Another perfect nanoencapsulation structure, nanocrystals-core@meso-shell,[18,19] provides nanoparticles with high dispersion, thermal stability, good mass-diffusion and molecule selectivity. Such an idea is elegant, although synthesis procedures are relatively complex and not easy to upgrade. Various special examples of nano-encapsulations, such as one particle@one cell[20] and one particle@ultrathin layer,[21] have been also synthesized by our group using a special window-cell meso-structure or a soluble polymer. It has to be noted that, for the nanoencapsulation,[22–27] the choice of meso-structures is mostly dependent on surface physicochemical properties and the size of the nanosized sites. This is a major reason why it is not easy to achieve success for all types of meso-structures using only one approach. It is therefore of great scientific interest and technological importance to develop a facile and versatile way to obtain highly dispersed nanometals within all types of meso-structured materials for enhanced catalytic activity and stability.

As is well known, the viscosity of the reaction solvent is the most basic and common synthesis factor, which plays an important role in the synthesis and dispersion of the nanocrystals. In general, a high-viscosity solvent seems to not be a good candidate, because of weak capillary inclusion, low ion-exchange efficiency and hard precursor impregnation. That is why low-viscosity solvents, especially highly volatile solvents such as water and alcohol, are often chosen as the carrier of the metal precursor into the mesochannels because of their fast diffusion and easy removal. However it also easily results in the formation of aggregates or assemblies of metal nanocrystals because of the fast random motion of metal nanoclusters in mesoporous supports. It is notable that high-viscosity solvents, *e.g.* 1,4-butanediol, have an ignored great advantage, which can slow down the random motion of metal nanoclusters and prevent the nanoclusters from aggregating during the formation of nanoclusters. For now it is a big blind spot in the synthesis of highly dispersed nanoparticles in mesoporous materials. Actually, short-time sonication can easily cover the problem of precursor impregnation, and lead to a homogeneous distribution of the precursor in the mesostructure. High viscosity might therefore be a more intelligent and desired option to highly dispersed nanometals. Herein, highly dispersed nanometals in mesostructured materials with different pore structures (2D (two-dimensional) and 3D (three-dimensional)), sizes (large and small) and compositions (silica and carbon) have

[a] *State Key Laboratory Advanced Technology for Materials Synthesis and Processing, Wuhan University of Technology, 122, Luoshi Road, Wuhan, 430070, China. E-mail: xyyang@whut.edu.cn*
[b] *EMAT (Electron Microscopy for Materials Science), University of Antwerp, Groenenborgerlaan 171, B-2020 Antwerpen, Belgium*
[c] *Institut für Anorganische Chemie und Strukturchemie, Heinrich-Heine-Universität Düsseldorf, 40204 Düsseldorf, Germany*
[d] *Laboratory of Inorganic Materials Chemistry (CMI), University of Namur, 61, rue de Bruxelles, B-5000 Namur, Belgium. E-mail: bao-lian.su@fundp.ac.be*

† Electronic supplementary information (ESI) available: Synthesis and SEM, TEM, XRD, $N_2$ ad/de data, CV and ORR curves. See DOI: 10.1039/c6cc00912c

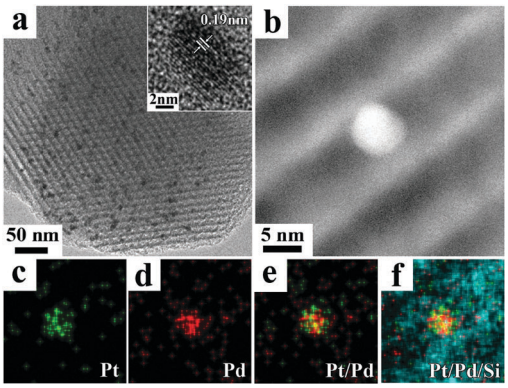


Fig. 1 (a) TEM image and (b) high magnification HAADF-STEM image of PtPd/SBA-15; (c–f) corresponding EDX elemental mapping results: (c) Pt, (d) Pd, (e) Pt and Pd, and (f) Pt, Pd and Si overlaid color mapping. Inset of (a) shows a high-magnification TEM image of an individual PtPd nanocrystal within PtPd/SBA-15.

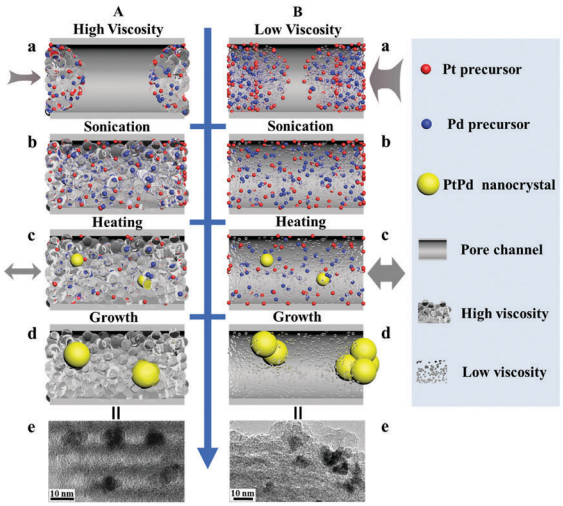


Fig. 2 Schematic illustration of the proposed formation mechanisms of nanometals synthesized in (A) high viscosity solvent and (B) low viscosity solvent: diffusion amounts and rates of metal precursors in different viscosity solvents (Aa and Ba); full impregnation of the reaction solution after sonication (Ab and Bb); forming of metal nanoclusters after heating (Ac and Bc); growth, dispersion (Ad) and aggregation (Bd) of nanocrystals and corresponding TEM images of PtPd/SBA-15 (Ae and Be). Arrows indicate directions and rates of mass exchange.

been synthesized by a viscosity-adjusting method. Very interestingly, these highly dispersed PtPd bimetallic nanoparticles exhibit a highly enhanced activity in various catalytic reactions such as hydrogenation and oxygen reduction.

SBA-15 was first used to highly disperse PtPd bimetallic nanocrystals (denoted as PtPd/SBA-15). Scanning electron microscopy (SEM) images of SBA-15 and PtPd/SBA-15 (Fig. S1, ESI†) show no change in the surface morphology, indicating that the porous framework of SBA-15 remains intact after supporting the PtPd nanocrystals. Transmission electron microscopy (TEM) images of PtPd/SBA-15 are shown in Fig. 1a. Nanocrystals with a uniform size of around 5 nm are highly dispersed in a large area of the SBA-15 support. The high-resolution TEM (HRTEM) image taken from a single nanocrystal shows well-defined fringes (inset of Fig. 1a), indicating the high crystalline nature of the PtPd nanocrystals. The lattice spacing of 0.19 nm is as expected for the (200) planes of the face centered cubic (fcc) PtPd alloy. Fig. 1b–f show high-angle annular dark-field scanning TEM (HAADF-STEM) images of an individual nanocrystal in the pore of SBA-15 and the corresponding energy-dispersive X-ray spectroscopy (EDX) mapping results. Pt and Pd elements are homogeneously distributed throughout the entire nanocrystal, as expected for a PtPd bimetallic nanocrystal with an intermetallic nanostructure. Moreover, the high-angle X-ray diffraction (XRD) patterns of SBA-15 and PtPd/SBA-15 (Fig. S2a, ESI†) show that the four observed peaks of PtPd/SBA-15 can be readily indexed to the (111), (200), (220) and (311) reflections of the fcc PtPd bimetallic nanocrystals, and the peaks are broadened because of the small size of PtPd nanocrystals. Compared to the typical peaks of Pd (JCPDS no. 05-0681), the four corresponding peaks of PtPd/SBA-15 are slightly shifted to lower 2 theta values, indicating expansion of the lattice parameters by the incorporation of Pt in the fcc structure of Pd.[28] These results strongly suggest that the nanocrystals are PtPd bimetallic nanocrystals. Meanwhile, the low-angle XRD patterns (Fig. S2b, ESI†), $N_2$ adsorption–desorption data (Fig. S3, ESI†) and physical parameters (Table S1, ESI†) of SBA-15 and PtPd/SBA-15 display the preservation of the ordered hexagonal mesoporous structure after supporting the metal nanocrystals. Notably, compared to SBA-15, the pore size, BET surface area, and pore volume of PtPd/SBA-15 are decreased. All these data suggest that the nanocrystals uniformly disperse into the mesochannels and do not block or destroy the meso-structure, which is very important for catalysis applications.

To better understand the formation mechanism of the highly dispersed PtPd nanoparticles in mesoporous supports, the effect of viscosity of the solvent in our reaction system was investigated in detail. Fig. 2 schematically shows the proposed formation mechanism of nanometals synthesized in a high viscosity solvent (Fig. 2A) and a low viscosity solvent (Fig. 2B). The starting precursors, mixed with a high viscosity solvent, are harder to impregnate into the mesochannels due to the weak capillary inclusion (Fig. 2Aa). After sonication, the precursor can infiltrate the mesochannels (Fig. 2Ab) and form nanoclusters by reduction (Fig. 2Ac). Then the nanoclusters grow in the relatively confined space because of the low exchange between inside and outside precursors. Furthermore, the mobility of the nanoclusters also decreases in a high viscosity solvent due to the weak Brownian motion (Fig. 2Ad). This might be a major reason why the metal nanocrystals individually grow and why aggregation does not occur. In contrast, the starting precursors in a low viscosity solvent can diffuse easily and fast into the mesochannels (Fig. 2Ba and b). At the same time, the internal–external exchange of precursors is facile and the random motion of nanoclusters is relatively fast, which means that the nanoclusters would easily aggregate (Fig. 2Bc and d). TEM results show the difference of PtPd/SBA-15 composites synthesized in a high viscosity solvent (1,4-butanediol, Fig. 2Ae and Fig. S4a, Table S2, ESI†) and a low viscosity solvent (ethylene glycol, Fig. 2Be and Fig. S4b, Table S2, ESI†) under otherwise similar synthesis conditions. It is evident

 

that the nanocrystals synthesized in high viscosity solvent are dispersed uniformly, while aggregation takes place when using a low viscosity solvent. Notably, these aggregates are composed of smaller primary nanocrystals with a size of around 5 nm, which are similar to the nanocrystals synthesized in 1,4-butanediol. This suggests that aggregation happens after the nanocluster formation and over-growth of nanocrystals might be rare. Further evidence is provided by the synthesis of nanometals using an even lower viscosity solvent (water; see TEM results of Fig. S4c and d, Table S2, ESI†). Even at the room temperature, metal aggregates with a bigger size of around 25 nm are formed in aqueous solution, in comparison with synthesis systems of ethylene glycol and 1,4-butanediol. Similarly, these aggregates are composed of primary nanocrystals with a size of around 5 nm, which further proves that the major problem associated with the dispersion of nanometals synthesized under certain conditions is the aggregation, not the over-growth. In other words, it is critical to decrease the mobility of the formed nanoclusters, especially during their growth stage of the nanoclusters. Moreover, when 1,4-butanediol is substituted with other high-viscosity solvents of 1,2-propanediol and 1,5-pentadiol, the reactions also yield uniform nanocrystals with a high dispersion (Fig. S4e and f, Table S2, ESI†). A high viscosity solvent therefore is the preferred choice, which can efficiently decrease the Brownian motion of nanoclusters and nanocrystals, even precursors.

As a comparison to a 2D mesoporous structure, MCF with a 3D mesoporous structure was used to support the PtPd bimetallic nanocrystals (denoted as PtPd/MCF). The PtPd bimetallic nanocrystals could be highly dispersed in the MCF and show a high crystallinity, which is clearly observed by the characterization of the TEM, HAADF-STEM and EDX (Fig. S5, ESI†). As a way of decreasing aggregation, the high viscosity method provides a good opportunity to highly disperse the nanometals onto mesoporous materials to avoid the aggregation outside the mesochannels. PtPd nanocrystals distributed onto the frameworks of the MCM-41 (denoted as PtPd/MCM-41) show high dispersion and intermetallic features (Fig. S6, ESI†). That further suggests that preparation of highly dispersed nanometals is a great advantageous feature of the high-viscosity solvent method, even if that the PtPd nanocrystals synthesized are outside of the pores of MCM-41. Also, both of mesostructures are retained according to the XRD and $N_2$ adsorption–desorption data (Fig. S7 and S8, ESI†). For comparison, the aggregates of small, primary metal nanocrystals supported by MCF (Fig. S9, ESI†) and MCM-41 (Fig. S10, ESI†) formed in low viscosity solvents of ethylene glycol and water are observed. Overviewing all the results of metal nanocrystals in/on various mesopores by the high viscosity solvent method, the core features can be shared: high dispersion and high crystallinity of metal nanocrystals, together with the good preservation of the pore ordering and porosity. The success for various mesostructured silica materials suggests that the high viscosity solvent method can be extended to the synthesis of highly dispersed nanometals in/on all types of nanoporous materials.

The hydrogenation of nitrobenzene as a model catalytic reaction was used to demonstrate their advantages and features

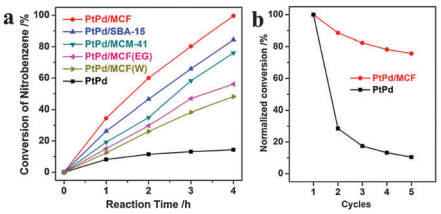


Fig. 3 (a) The time-domain conversion of nitrobenzene by different PtPd catalysts. (b) A comparison of conversion for PtPd/MCF and PtPd during the five reaction cycles. The reaction time is 4 h.

in catalysis. For comparison, PtPd nanocrystals within MCF synthesized in ethylene glycol (denoted as PtPd/MCF(EG)), water (denoted as PtPd/MCF(W)), and PtPd nanocrystals synthesized in 1,4-butanediol (denoted as PtPd) were also used as references. As shown in Fig. 3a, the catalytic efficiencies of all samples show a clear and similar tendency at different times, which is PtPd/MCF > PtPd/SBA-15 > PtPd/MCM-41 > PtPd/MCF(EG) > PtPd/MCF(W) > PtPd. Taking 4 h as an example (see Table S3, ESI†), the conversions of nitrobenzene for PtPd/MCF, PtPd/SBA-15, PtPd/MCM-41, PtPd/MCF(EG), PtPd/MCF(W) and PtPd are 99.6%, 84.5%, 76.1%, 56.2%, 48.2%, and 14.4%, respectively. The normalized turnover frequencies (TOFs) are also in agreement with the conversions. For instance, the TOF of PtPd/MCF (4.98 mol $g^{-1}$ $h^{-1}$) is about 6.9 times greater than that of PtPd (0.72 mol $g^{-1}$ $h^{-1}$). It is noteworthy that PtPd/MCF shows a high catalytic activity and stability during the recycle test. For example, after 5 recycles, PtPd/MCF still exhibits 75.6% of the initial activity (Fig. 3b), while only 10.4% is shown by free PtPd. The porous structure and the surface area of PtPd/MCF show no obvious change and a slight natural loss of the PtPd loading amount occurs (Fig. S11 and Table S4, ESI†), indicating high stability of this composite obtained. There are several features to be noted. First, the catalytic activities of supported PtPd are higher than that of PtPd without support, which can be ascribed to the organic capping,[29] solvent-stability, and the high surface area of the mesoporous supports. Second, the PtPd/mesoporous silica samples using the high-viscosity solvent show higher catalytic performances than the PtPd/mesoporous silica synthesized in the low-viscosity solvent, which can be attributed to smaller-scale nanocrystals and their better dispersion in the mesostructures. Third, PtPd/large-sized mesopores (PtPd/MCF and PtPd/SBA-15) present superior catalytic activities, compared with PtPd/small-sized mesopores (PtPd/MCM-41), which is due to more exposed active sites and/or active facets in this case. Finally, the PtPd/3D mesostructure (PtPd/MCF) has the best catalytic performance of all tested samples. This could be attributed to the 3D structure and the largest pore system of MCF, which results in better mass diffusion and more exposed active sites and/or active facets compared to a 2D mesostructure.

With further extension, PtPd bimetallic nanocrystals within mesoporous carbon of CMK-3 (denoted as PtPd/CMK-3) are therefore synthesized by the high viscosity solvent method, and evaluated by electrocatalysis. The procedure for synthesis of PtPd/CMK-3 is similar to that of PtPd/silica, except that mesoporous silica is substituted by CMK-3. Similar data of PtPd/CMK-3 are

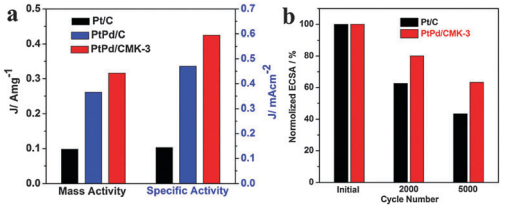


Fig. 4 (a) Mass activity and specific activity at 0.9 V *versus* RHE for commercial Pt/C, PtPd/C and PtPd/CMK-3. (b) Loss of ECSA of commercial Pt/C and PtPd/CMK-3 after potential sweep cycles.

shown. The representative TEM (Fig. S12, ESI†) image reveals that highly crystalline nanocrystals are well dispersed in the CMK-3. The low- and high-angle XRD patterns of PtPd/CMK-3 (Fig. S13, ESI†) indicate the preservation of the pore structure after nanoparticle deposition, a good crystalline degree and the PtPd intermetallic nature of the particles. The preservation of the pore structure of CMK-3 and the introduction of PtPd nanocrystals can be further demonstrated by comparing the $N_2$ adsorption–desorption data of CMK-3 and PtPd/CMK-3 (Fig. S14, ESI†). Considering the good electroconductivity of PtPd/carbon-based materials, we also evaluated the electrocatalytic properties of PtPd/CMK-3 toward the oxygen reduction reaction (ORR) against PtPd/C and the commercial Pt/C catalyst (Table S5, ESI†). Fig. S15 (ESI†) shows the cyclic voltammetry (CV) curves and the ORR polarization curves of the three catalysts. The electrochemically active surface area (ECSA) of PtPd/CMK-3 (53.3 $m^2\ g^{-1}$) is calculated to be about 78% of the Pt/C catalyst (68.2 $m^2\ g^{-1}$), and is comparable with PtPd/C (55.5 $m^2\ g^{-1}$). As shown in Fig. 4a, the mass activity and specific activity of PtPd/CMK-3 (0.316 A $mg^{-1}$ and 0.594 mA $cm^{-2}$) are about 3.1 and 4.1 times greater than that of Pt/C (0.101 A $mg^{-1}$ and 0.144 mA $cm^{-2}$), which demonstrates the superior electrocatalytic properties of PtPd/CMK-3 toward the ORR. PtPd/CMK-3 shows a higher catalytic activity than PtPd/C and Pt/C, demonstrating the structural superiority and the nano-alloying effect in electrocatalysis. Further, the PtPd/CMK-3 shows high durability and exhibits a loss of 36.7% after 5000 cycles, which is higher than Pt/C (56% of loss) (Fig. 4b). The good electrocatalytic performance of PtPd/CMK-3 can be attributed to the nanoalloying effect and the high dispersion of the nanometals.

In conclusion, we have developed a facile and general approach to synthesize highly dispersed metal nanocrystals within various mesostructures *via* the high viscosity solvent method. The features of the highly dispersed nanometals have been further proven in hydrogenation and oxygen reduction. It is believed that our method can potentially be extended to the design and preparation of highly dispersed heterogeneous catalysts with excellent performance.

This work was supported by NFSC (51472190 and 51503166), ISTCP (2015DFE52870), PCSIRT (IRT_15R52) of China, and the Integrated Infrastructure Initiative of EU (312483-ESTEEM2).

## Notes and references

1 X. Ji, K. T. Lee, R. Holden, L. Zhang, J. Zhang, G. A. Botton, M. Couillard and L. F. Nazar, *Nat. Chem.*, 2010, **2**, 286–293.
2 J. Sun, A. M. Karim, X. S. Li, J. Rainbolt, L. Kovarik, Y. Shin and Y. Wang, *Chem. Commun.*, 2015, **51**, 16617–16620.
3 D. Wang, B. Ma, B. Wang, C. Zhao and P. Wu, *Chem. Commun.*, 2015, **51**, 15102–15105.
4 F. Colbeau-Justin, C. Boissière, A. Chaumonnot, A. Bonduelle and C. Sanchez, *Adv. Funct. Mater.*, 2014, **24**, 233–239.
5 C. Chen, J. Zhu, F. Chen, X. Meng, X. Zheng, X. Gao and F.-S. Xiao, *Appl. Catal., B*, 2013, **140**, 199–205.
6 G. Prieto, J. Zečević, H. Friedrich, K. P. de Jong and P. E. de Jongh, *Nat. Mater.*, 2013, **12**, 34–39.
7 P. Z. Li, A. Aijaz and Q. Xu, *Angew. Chem., Int. Ed.*, 2012, **51**, 6753–6756.
8 A. Aijaz, A. Karkamkar, Y. J. Choi, N. Tsumori, E. Rönnebro, T. Autrey, H. Shioyama and Q. Xu, *J. Am. Chem. Soc.*, 2012, **134**, 13926–13929.
9 J. Ying, X.-Y. Yang, G. Tian, C. Janiak and B.-L. Su, *Nanoscale*, 2014, **6**, 13370–13382.
10 S.-H. Liu, R.-F. Lu, S.-J. Huang, A.-Y. Lo, S.-H. Chien and S.-B. Liu, *Chem. Commun.*, 2006, 3435–3437.
11 F. Su, F. Y. Lee, L. Lv, J. Liu, X. N. Tian and X. S. Zhao, *Adv. Funct. Mater.*, 2007, **17**, 1926–1931.
12 H. Liu, D. Ma, R. A. Blackley, W. Zhou and X. Bao, *Chem. Commun.*, 2008, 2677–2679.
13 A. K. Prashar, R. P. Hodgkins, R. Kumar and R. N. Devi, *J. Mater. Chem.*, 2008, **18**, 1765–1770.
14 B. F. Johnson, *Top. Catal.*, 2003, **24**, 147–159.
15 K. B. Lee, S. M. Lee and J. Cheon, *Adv. Mater.*, 2001, **13**, 517–520.
16 J. Sun, D. Ma, H. Zhang, X. Liu, X. Han, X. Bao, G. Weinberg, N. Pfänder and D. Su, *J. Am. Chem. Soc.*, 2006, **128**, 15756–15764.
17 L. Li, J. L. Shi, L. X. Zhang, L. M. Xiong and J. N. Yan, *Adv. Mater.*, 2004, **16**, 1079–1082.
18 S. H. Joo, J. Y. Park, C.-K. Tsung, Y. Yamada, P. Yang and G. A. Somorjai, *Nat. Mater.*, 2009, **8**, 126–131.
19 X.-Y. Yang, Y. Li, G. Van Tendeloo, F.-S. Xiao and B.-L. Su, *Adv. Mater.*, 2009, **21**, 1368–1372.
20 J. Ying, X.-Y. Yang, Z.-Y. Hu, S.-C. Mu, C. Janiak, W. Geng, M. Pan, X. Ke, G. Van Tendeloo and B.-L. Su, *Nano Energy*, 2014, **8**, 214–222.
21 K. Cheng, Z. Kou, J. Zhang, M. Jiang, H. Wu, L. Hu, X.-Y. Yang, M. Pan and S. Mu, *J. Mater. Chem. A*, 2015, **3**, 14007–14010.
22 X.-Y. Yang, Z.-Q. Li, B. Liu, A. Klein-Hofmann, G. Tian, Y.-F. Feng, Y. Ding, D. S. Su and F.-S. Xiao, *Adv. Mater.*, 2006, **18**, 410–414.
23 P. C. Angelomé, I. Pastoriza-Santos, J. Pérez-Juste, B. Rodríguez-González, A. Zelcer, G. J. Soler-Illia and L. M. Liz-Marzán, *Nanoscale*, 2012, **4**, 931–939.
24 T. Bian, L. Shang, H. Yu, M. T. Perez, L. Z. Wu, C. H. Tung, Z. Nie, Z. Tang and T. Zhang, *Adv. Mater.*, 2014, **26**, 5613–5618.
25 J. Yang, H. Zhang, M. Yu, I. Emmanuelawati, J. Zou, Z. Yuan and C. Yu, *Adv. Funct. Mater.*, 2014, **24**, 1354–1363.
26 N. Jiang, X.-Y. Yang, G.-L. Ying, L. Shen, J. Liu, W. Geng, L.-J. Dai, S.-Y. Liu, J. Cao and G. Tian, *Chem. Sci.*, 2015, **6**, 486–491.
27 N. Jiang, X. Y. Yang, Z. Deng, L. Wang, Z. Y. Hu, G. Tian, G. L. Ying, L. Shen, M. X. Zhang and B. L. Su, *Small*, 2015, **11**, 2003–2010.
28 H. Li, Q. Xin, W. Li, Z. Zhou, L. Jiang, S. Yang and G. Sun, *Chem. Commun.*, 2004, 2776–2777.
29 H. Lee, S. E. Habas, S. Kweskin, D. Butcher, G. A. Somorjai and P. Yang, *Angew. Chem., Int. Ed.*, 2006, **45**, 7824–7828.

 